Chapter 2

Direct-coupled array of qubits

In this and next chapter we study the nonlinear transport of photons through lattices made of qubits and resonators. The established approach for quantum theory of such systems is that of open quantum systems developed within the context of quantum optics. We first describe the general formalism briefly before applying it to our systems.

2.1 Open quantum systems

To study the transmission of light through systems considered in this thesis, a source of light (photons) is connected from one end (left) using a laser or a microwave generator depending on the experimental system and observe them at the other end of the system with a suitable detector. The input source injects photons into the medium which is observed at the other end namely output, and characterizes the system it has traversed. In the physical realizations of these systems, the waveguides made of line-defect photonic crystals or transmission lines are much longer than the typical wavelength of photons employed in that experiment. Thus, the waveguide can be treated as infinitely long. Nevertheless, the length of the systems in our effective theoretical modeling is finite and is the same as the number of qubits or resonators. In our studied Hamiltonians, the sources and detectors are modeled as the left and right baths respectively.

The entire system including the baths is described by the Hamiltonian

$$H = H_M + H_{LB} + H_{RB} + H_{LM} + H_{RM}, \tag{2.1}$$

where H_M represents the Hamiltonian of the medium which, in this and next chapter, are the direct-coupled qubits (H_{direct}) and resonator chain with side-coupled qubits (H_{side})

respectively. H_{LB} (H_{RB}) is the left (right) bath and H_{LM} (H_{RM}) is the coupling between the chain and the left (right) bath. The bath and the bath-medium coupling Hamiltonians within the Markov and rotating-wave approximations are [Manasi and Roy, 2018]

$$H_{LB(RB)} = \int_{-\infty}^{+\infty} dk\, \hbar\omega_k a^{\dagger}_{Lk(Rk)} a_{Lk(Rk)}, \tag{2.2}$$

$$H_{LM} = \int_{-\infty}^{+\infty} dk\, \hbar g_L (a^{\dagger}_{Lk}\chi_1 + \chi_1^{\dagger} a_{Lk}), \tag{2.3}$$

$$H_{RM} = \int_{-\infty}^{+\infty} dk\, \hbar g_R (a^{\dagger}_{Rk}\chi_N + \chi_N^{\dagger} a_{Rk}). \tag{2.4}$$

The operators $a^{\dagger}_{Lk}$ and $a^{\dagger}_{Rk}$ are the creation operators with wave number k in the left and right side baths respectively. We set the ground state energy of the bath to be zero and have $[a_{Lk'}, a^{\dagger}_{Lk}] = [a_{Rk'}, a^{\dagger}_{Rk}] = \delta(k-k')$. The bosonic operators χ_1 and χ_N correspond to the left and right most qubits / resonators of the medium, which are coupled to the baths with strengths g_L and g_R respectively. We use $\chi_j = b_j$ (f_j) for a direct-coupled (side-coupled) array of qubits (see below). Both the baths contain left- and right-moving photons; hence k can take both positive and negative values representing photons moving towards right and left respectively. However, because of our particular initial condition only right-moving photons for the right baths are relevant. Here, we assume a linear energy-momentum dispersion relation for the two baths, i.e., $\omega_k = v_g|k|$ with v_g being the group velocity of photons. The k-independent couplings g_L and g_R within the Markov approximation ensure that we can turn a set of integro-differential Heisenberg-Langevin equations for qubit variables into a set of differential equations (see Sec. 2.3).

The baths are kept at a temperature of 0K to ensure a coherent light source. At time t_0 the medium-bath coupling is switched on and incoming light interacts with the ends of the chain. For a weak bath-medium coupling, we write the H_{LM} and H_{RM} within the rotating wave approximation where we drop the counter rotating terms. Assuming that a coherent light is incident from the left and the initial state (at $t = t_0$) for the coherent light source is $|E_p, \omega_p\rangle$,

$$a_{Lk}(t_0)|E_p, \omega_p\rangle = E_p \delta(v_g k - \omega_p)|E_p, \omega_p\rangle, \tag{2.5}$$

$$a_{Rk}(t_0)|E_p, \omega_p\rangle = 0, \tag{2.6}$$

where E_p is the amplitude of the incoming light while ω_p is its frequency. The initial condition converts the noises from the bath into the Rabi frequency of the system, given by $\Omega_L = g_L E_p / v_g$, and medium-bath coupling rates from the left and right baths given by, $\Gamma_L = \pi g_L^2 / v_g$ and $\Gamma_R = \pi g_R^2 / v_g$ respectively. The noise terms can now be replaced in the quantum Langevin equations for the qubits / resonators with these constant terms. The Rabi frequency appears in the system of equations either as a constant source term or as prefactors to certain operators, while the bath-medium coupling rates only appear as the latter. The incoming photon frequency (ω_p) appears as time-dependent phase factors in the quantum Langevin equations which are absorbed by suitable redefinition of the operators.

2.2 Model

A simple Bose-Hubbard type model system that shows correlated light propagation is a 1D array of qubits with direct coupling between nearest neighbors [Schmidt and Koch, 2013; Naether et al., 2015b; Ma et al., 2019]:

$$H_M = H_{direct} = \sum_{j=1}^{N} \hbar\omega_{q_j} b_j^\dagger b_j + \hbar U b_j^\dagger b_j (b_j^\dagger b_j - 1) + \sum_{j=1}^{N-1} 2\hbar J_x (b_j^\dagger b_{j+1} + b_{j+1}^\dagger b_j). \quad (2.7)$$

Here, $b_j^\dagger$ and b_j are the bosonic creation and annihilation operators at site j with ω_{q_j} being the qubit frequency and $[b_i, b_j^\dagger] = \delta_{i,j}$. The direct-coupled medium is coupled to the two baths through $\chi_1 = b_1$ and $\chi_N = b_N$. $2J_x$ is the coupling strength between neighboring qubits. U determines the strength of on-site interaction, which is repulsive for positive U. In the limit $U \to \infty$, the qubit maps to a two-level system. The on-site interaction at the qubits induces optical nonlinearity in the model by preventing multiple excitations by photons, and is responsible for the inelastic light scattering studied in this work.

2.2.1 Integrating out the baths

Following [Manasi and Roy, 2018], we first integrate out the baths. The Heisenberg equations for the photon operators of the bath, a_{Lk} and a_{Rk} are inhomogeneous linear differential equations. The initial condition (at $t = t_0$) will set the direction of the incoming light in the system. By solving the Heisenberg equations for the baths, we obtain the time evolution of the bath operators [Manasi and Roy, 2018] given by,

$$a_{Lk}(t) = \mathscr{G}_k(t-t_0) a_{Lk}(t_0) - i g_L \int_{t_0}^{t} dt' \mathscr{G}_k(t-t') \chi_1(t'), \quad (2.8)$$

$$a_{Rk}(t) = \mathscr{G}_k(t-t_0) a_{Rk}(t_0) - i g_R \int_{t_0}^{t} dt' \mathscr{G}_k(t-t') \chi_N(t'), \quad (2.9)$$

where, $\mathscr{G}_k(\tau) = \theta(\tau) e^{-i v_g k \tau}$ is the retarded Green's function of the baths. The bath solutions, Eqs. 2.8-2.9, are substituted in the remaining equations of motion for the qubits and give rise to the noise operators due to the baths which are given as, $\eta_L(t) = \int_{-\infty}^{\infty} dk \mathscr{G}_k(t - t_0) g_L a_{Lk}(t_0)$ and $\eta_R(t) = \int_{-\infty}^{\infty} dk \mathscr{G}_k(t - t_0) g_R a_{Rk}(t_0)$. These noises coming from the baths can be converted to constant numbers by considering an appropriate initial condition.

2.3 Analysis

2.3.1 Truncated Heisenberg-Langevin equations

As the qubits are bosonic, each of them can have any number of excitations. These excited states appear as powers of b_j and $b_j^\dagger$ in the operators. To describe the THLE, we need to consider every independent boson operator for each qubit for each site; which are $\{I, b_j, b_j^\dagger, b_j^\dagger b_j, b_j^2, b_j^{\dagger 2}, b_j^\dagger b_j^2, b_j^{\dagger 2} b_j, b_j^{\dagger 2} b_j^2, ...\}$. However, as there are infinite number of possible operators, we must truncate the set of boson operators. If we restrict our system to have only one excitation, then only the first four of these operators would enter the equations. In this case, for example, to obtain the set of equations for two qubits we consider every operator in the set $\{I, b_1, b_1^\dagger, b_1^\dagger b_1\} \otimes \{I, b_2, b_2^\dagger, b_2^\dagger b_2\}$, which gives 16 independent operators. The operator $I \otimes I$ is ignored as it has no dynamics and we are left with 15 operators. The number of operators increases exponentially as number of qubits (N) increases and are given by $\{I, b_j, b_j^\dagger, b_j^\dagger b_j\}^{\otimes N}$.

Including more excited states in our operator set will increase the accuracy of the results, however, for relatively high on-site interaction (U), appropriate accuracy can be achieved by considering a limited number of excited states. As more excited states per site (m) are included, the number of operators increases with a polynomial growth where the exponent is $2N$, we denote m as maximum number of bosons per site. For example, if $m = 2$, the number of operators for a chain of two qubits $(N = 2)$ increases to 80 as the operator set becomes $\{I, b_j, b_j^\dagger, b_j^\dagger b_j, b_j^2, b_j^{\dagger 2}, b_j^2 b_j^\dagger, b_j b_j^{\dagger 2}, b_j^2 b_j^{\dagger 2}\}^{\otimes 2}$. Similarly, for a chain with N qubits with m allowed excited states per site, we shall get $(m+1)^{2N} - 1$ operators.

We illustrate the THLE analysis by writing the equations of motion for the simplest system considered here, namely a single qubit. The expectation values of qubit operators after integrating the baths from the equations along with its phase factor are denoted as,

$$\mathscr{S}_{kl} = \langle b_1^{\dagger k} b_1^l \rangle e^{(-k+l) i \omega_p (t - t_0)}, \tag{2.10}$$

where the phase factor has been chosen such that the RHS of the equations of motion have no explicit time dependence. A few examples can be, $\mathscr{S}_{01} = \langle b_1 \rangle e^{i \omega_p (t - t_0)}$, $\mathscr{S}_{22} = \langle b_1^{\dagger 2} b_1^2 \rangle$. Applying this convention to our equations, and setting $m = 2$, we get the following set of eight coupled differential equations:

$$\dot{\mathscr{S}}_{01} = -(i\delta\omega_{q_1} + \Gamma_L + \Gamma_R)\mathscr{S}_{01} - 2iU\mathscr{S}_{12} - i\Omega_L, \tag{2.11}$$

$$\dot{\mathscr{S}}_{02} = -(\delta\omega_{q_1} + 2\Gamma_L + 2\Gamma_R)\mathscr{S}_{02} - 2iU(\mathscr{S}_{02} + 2\mathscr{S}_{13}) - 2i\Omega_L\mathscr{S}_{01}, \tag{2.12}$$

$$\dot{\mathscr{S}}_{11} = -2(\Gamma_L + \Gamma_R)\mathscr{S}_{11} - i\Omega_L(\mathscr{S}_{10} - \mathscr{S}_{01}), \tag{2.13}$$

$$\dot{\mathscr{S}}_{12} = -(i\delta\omega_{q_1} + 3\Gamma_L + 3\Gamma_R)\mathscr{S}_{12} - 2iU(\mathscr{S}_{12} + \mathscr{S}_{23}) - i\Omega_L(2\mathscr{S}_{11} - \mathscr{S}_{02}), \tag{2.14}$$

$$\dot{\mathscr{S}}_{22} = 2(2\Gamma_L + 2\Gamma_R)\mathscr{S}_{22} - i\Omega_L(2\mathscr{S}_{21} - 2\mathscr{S}_{12}). \tag{2.15}$$

here, $\delta\omega_{q_1} = \omega_{q_1} - \omega_p$ and the remaining equations are the hermitian conjugates of the equations 2.11, 2.12 and 2.14. In the truncation scheme with $m = 2$, we ignore all other equations with higher values of k, l in Eq. 2.10. Note that we still get the operators we have ignored due to the truncation on the RHS of the above equation for example in Eqs. 2.12-2.14 and their hermitian conjugates. We drop these terms in the further analysis, and explicitly check the accuracy of the truncation by considering various values of m. As mentioned before, increasing m increases accuracy of the results but also expands the set of equations.

The equations 2.11-2.15, and their hermitian conjugates, can be re-written in a matrix form with the vectors $\mathscr{S}(t) = \{\mathscr{S}_{01}, \mathscr{S}_{02}, \mathscr{S}_{10}, \mathscr{S}_{11}, \mathscr{S}_{12}, \mathscr{S}_{20}, \mathscr{S}_{21}, \mathscr{S}_{22}\}^T$ and $\Omega = \{-i\Omega_L, 0, i\Omega_L, 0, 0, 0, 0, 0\}^T$. The linear system of equations can be represented very compactly as

$$\dot{\mathscr{S}}(t) = \mathscr{Z}\mathscr{S}(t) + \Omega. \tag{2.16}$$

We analyse the models using the Heisenberg-Langevin equations which is an exact calculation method for an open quantum system within the Markovian approximation [Scully and Zubairy, 1997b; Roy et al., 2017; Manasi and Roy, 2018]. Since each component is modeled as harmonic or anharmonic oscillators the local Hilbert space is infinite dimensional. As a result we necessarily have to perform a truncation in any numerical calculation. This truncation is a further approximation whose correctness is checked explicitly by considering various degree of truncation. Assuming the qubits in the ground state before irradiation with photon, we solve the coupled set of equations to get the steady-state results, which occurs when $t \gg t_0$ after some transient time. We obtain the long-time ($t \to \infty$) steady-state solution by solving $\frac{d\mathscr{S}(t)}{dt} = 0$, which gives the time independent solution of the equations as $\mathscr{S}(t \to \infty) = -\mathscr{Z}^{-1}\Omega$.

2.3.2 The quasi-classical analysis

The models studied here can also be investigated using a quasi-classical system of equations, which are obtained by the classical limit approximation where the operators are replaced by their averages ($\langle b_j \rangle = \beta_j$) for e.g. $\langle b_j^\dagger b_j^2 \rangle = |\beta_j|^2 \beta_j$ [Naether et al., 2015a]. This approximation limits the set of equations in their first moment. For the direct-coupled qubits system, we obtain

$$\dot{\beta}_j = -(i\delta\omega_{q_j} + \Gamma_j)\beta_j - 2iU|\beta_j|^2\beta_j - 2iJ_x(\beta_{j-1} + \beta_{j+1}) - i\Omega_L \delta_{1,j}, \tag{2.17}$$

where, $\Gamma_j = 0$ for $2 \le j \le N-1$, $\Gamma_1 = \Gamma_L$ and $\Gamma_N = \Gamma_R$. If $N = 1$, $\Gamma = \Gamma_L + \Gamma_R$. We use open boundary condition for the medium, i.e., $\beta_0 = \beta_{N+1} = 0$.

These equations are solved using standard numerical differential equation solvers to obtain the long-time steady-state solutions. At very low intensities when the interaction and non-linearity in the system are not significant, the QCA has a perfect agreement with the THLE results. However, with increasing intensity, the QCA fails to capture any effects of inelastic scattering of the photons as predicted by the THLE analysis. The peaks in transmission profile calculated using QCA starts shifting towards higher frequencies as the intensity is increased. This drastic failure of QCA is possibly a reflection of the fact that the approximation is missing the inelastic scattering of the photons due to interaction. If we consider the Eq. 2.17 carefully we realize that the interaction term is contributing as extra occupation dependent contribution to the oscillation frequency instead of a term that can cause a decrease in oscillation amplitude. The blockade phenomena should have contributed the latter. In particular, for the QCA, there is always some frequency that has perfect transmission. In the case where input intensity is very high, the shift can be so large that the peak may go outside the range of input frequencies considered and it can be mistakenly interpreted as very low transmission caused by interaction.

The non-linearity in the QCA due to on-site interaction term can cause more than one steady-states, e.g., a multi-stability in the system which is absent in the present THLE analysis with one-time variables. It is also possible to find stable oscillating solutions for these quasi-classical equations. These non-linear features of the quasi-classical equations appear at high intensities, while the QCA begins to fail even at much lower intensity. We also carried out a self-consistent mean-field analysis of the system (subsection 2.3.5) but it also fails to capture the inelastic scattering of the photons at higher intensities. Interestingly, both the approximate analyses, namely QCA and self-consistent mean-field, give the same incorrect results for a wide range of parameters.

2.3.3 Modified quasi-classical equations

In contrast to THLE analysis, the quasi-classical equations can be solved very easily as there are only N equations involved. The quasi-classical equations increase linearly with system size N and hence enables us to analyze number of system with hundreds of qubits. A careful analysis of the quasi-classical equations reveals that the above mentioned shift in the transmission profile is due to the on-site interaction term (U). We observe that we need to incorporate inelastic scattering of the photons and related reduction in the transmission within the QCA. To highlight the fact that this inelastic scattering of the photons and the related reduction in photon transmission are caused due to interaction, we modify the interaction parameter U to become a complex number (U_{eff}). We choose its value to match the THLE analysis results for the single qubit case.

To calculate U_{eff} for the direct-coupled qubits, we consider a truncated system of five operators $S^T = \left[\mathscr{S}_{01} \quad \overline{\mathscr{S}_{01}} \quad \mathscr{S}_{11} \quad \mathscr{S}_{12} \quad \overline{\mathscr{S}_{12}}\right]$ and calculate their THLE which are given by Eqs. 2.11, 2.13, 2.14 and the conjugates of Eqs. 2.11, 2.14.

By solving Eqs. 2.13 and 2.14, we obtain the steady-state values $\mathscr{S}_{11}^{\infty}$ and $\mathscr{S}_{01}^{\infty}$ in terms of $\mathscr{S}_{01}^{\infty}$

$$\mathscr{S}_{11}^{\infty} = \frac{i\Omega_L\left(\mathscr{S}_{01}^{\infty} - \overline{\mathscr{S}_{01}^{\infty}}\right)}{2\Gamma}, \tag{2.18}$$

$$\mathscr{S}_{12}^{\infty} = \frac{\Omega_L^2\left(\mathscr{S}_{01}^{\infty} - \overline{\mathscr{S}_{01}^{\infty}}\right)}{\Gamma\left(i(\delta\omega_{q_1} + 2U) + 3\Gamma\right)}, \tag{2.19}$$

where, $\Gamma = \Gamma_L + \Gamma_R$. The steady-state solutions are substituted in Eq. 2.11 at steady-state which gives

$$\mathscr{S}_{01}^{\infty}\left(-\Gamma - i\delta\omega_{q_1}\right) - \frac{2iU\Omega_L^2\left(\mathscr{S}_{01}^{\infty} - \overline{\mathscr{S}_{01}^{\infty}}\right)}{\Gamma\left(i(\delta\omega_{q_1} + 2U) + 3\Gamma\right)} - i\Omega_L = 0, \tag{2.20}$$

The Eq. 2.20 can be re-written in real and imaginary parts of $\mathscr{S}_{01}^{\infty}$ by substituting $\mathscr{S}_{01}^{\infty} = S_x + iS_y$ which gives two equations for the two real variables. We solve these two equations to obtain steady-state values of S_x and S_y as Eqs. 2.21 and 2.22.

$$S_x = -\frac{\Omega_L\left((\delta\omega_{q_1} + 2U)^2\delta\omega_{q_1} + 12U\Omega_L^2 + 9\Gamma^2\delta\omega_{q_1}\right)}{(\delta\omega_{q_1} + 2U)^2\left(\Gamma^2 + \delta\omega_{q_1}^2\right) + 4(\delta\omega_{q_1} + 2U)U\Omega_L^2 + 12U\Omega_L^2\delta\omega_{q_1} + 9\Gamma^4 + 9\Gamma^2\delta\omega_{q_1}^2} \tag{2.21}$$

$$S_y = -\frac{\Gamma\Omega_L\left((\delta\omega_{q_1}+2U)^2+9\Gamma^2\right)}{(\delta\omega_{q_1}+2U)^2\left(\Gamma^2+\delta\omega_{q_1}^2\right)+4(\delta\omega_{q_1}+2U)U\Omega_L^2+12U\Omega_L^2\delta\omega_{q_1}+9\Gamma^4+9\Gamma^2\delta\omega_{q_1}^2}. \tag{2.22}$$

For comparison with the QCA at steady-state, the quasi-classical equation for the medium of single qubit is given as

$$-2iU|\beta_1^{ss}|^2\beta_1^{ss} - i\Omega_L + \beta_1^{ss}\left(-\Gamma - i\delta\omega_{q_1}\right) = 0. \tag{2.23}$$

The transmission probability for the THLE and QCA for $N = 1$ at steady-state is given by

$$\mathscr{T}_{\text{THLE}} = \frac{2\Gamma_R}{v_g I_{\text{in}}}\mathscr{S}_{11}^{\infty}, \tag{2.24}$$

$$\mathscr{T}_{\text{QCA}} = \frac{2\Gamma_R}{v_g I_{\text{in}}}|\beta_1^{ss}|^2. \tag{2.25}$$

In order to match these transmission probabilities for the THLE steady-state obtained above with the QCA steady-state, we obtain the magnitude of β_1^{ss} by demanding that the transmission obtained in the two calculations are the same, which gives

$$|\beta_1^{ss}|^2 = \mathscr{S}_{11}^{\infty} = -\frac{S_y\Omega_L}{\Gamma}. \tag{2.26}$$

Comparing transmission, however, does not give us the phase of β_1^{ss} but we choose it to be the same as that of $\mathscr{S}_{01}^{\infty}$ which yields

$$\beta_{1,r}^{ss} = \frac{|\beta_1^{ss}|S_x}{\sqrt{S_x^2+S_y^2}} \qquad \beta_{1,i}^{ss} = \frac{|\beta_1^{ss}|S_y}{\sqrt{S_x^2+S_y^2}}, \tag{2.27}$$

where $\beta_{1,r}^{ss}$ and $\beta_{1,i}^{ss}$ are the real and imaginary parts of β_1^{ss} and $|\beta_1^{ss}| = \sqrt{(\beta_{1,r}^{ss})^2+(\beta_{1,i}^{ss})^2}$.

Finally, we re-define the U as U_{eff} and re-arrange Eq. 2.23 to obtain

$$U_{\text{eff}} = \frac{-\Omega_L + \beta_1^{ss}\left(i\Gamma - \delta\omega_{q_1}\right)}{2|\beta_1^{ss}|^2\beta_1^{ss}}. \tag{2.28}$$

For a single qubit, we find almost perfect agreement between THLE and the modified QCA from its inception, apart from small deviations due to truncation error. Quite remarkably, we find that the modified equations work well even for longer chains. The advantage of using quasi-classical equations lies in its simplicity and computational efficiency, which enables us to study the transmission for much longer system sizes which are computationally more challenging.

As U_{eff} was calculated using the single site case for the media, it does not depend on J_x. Nevertheless, we find a good agreement between the THLE and modified QCA for greater system sizes as long as relatively low values of J_x $(< \Gamma_L = \Gamma_R)$ are used. However, an increase in J_x causes disagreements between the THLE and modified QCA. Albeit, the corrected QCA gives quite useful results for a good range of parameters.

For the direct-coupled qubit array, within the limited system sizes that we could explore using the THLE analysis, we find very little system size dependence of the resonant transmission. This suggests that the inelastic scattering of the photons and photon transmission reduction caused by on-site interactions seem to be dominated at the two ends. This is also consistent with earlier studies on two level atoms in absence of nearest neighbor interactions [Manasi and Roy, 2018]. However, we end up causing too much of inelastic scattering of the photons and transmission reduction using a homogeneous complex on-site interaction everywhere in the modified QCA. In fact, the resonant transmission for a homogeneous complex on-site interaction decreases with increasing system size and eventually falls to zero. This mismatch can be surmounted by applying complex on-site interaction only at the two ends of the medium while using its real part in the bulk of the chain. With this fix, we obtain system size independent transmission upto a chain of 300 qubits.

2.3.4 Transmission probability for the medium

To obtain the output transmission from the right end of the medium, we calculate the solutions of the coupled differential equations in the THLE analysis for the medium. The intensity of incoming light from the left side of the medium is I_{in} $(= E_p^2/2\pi v_g^2)$. For the direct-coupled qubit medium, the transmission probability, at time t, for a medium of N qubits is given as

$$\mathscr{T}_{\text{THLE}}(t) = \frac{2\Gamma_R}{v_g I_{\text{in}}} \langle b_N^\dagger b_N \rangle, \tag{2.29}$$

where $\langle b_N^\dagger b_N \rangle$ is the number operator expectation value at the output qubit. We can similarly obtain the QCA transmission probability by calculating the expectation value of the qubit operator β_N from the QCA. The QCA transmission probability is given as

$$\mathscr{T}_{\text{QCA}}(t) = \frac{2\Gamma_R}{v_g I_{\text{in}}} \beta_N^*(t)\beta_N(t). \tag{2.30}$$

The reflection probability in the THLE is given by

$$\mathscr{R}_{\text{THLE}}(t) = 1 + \frac{2\Omega_L}{v_g I_{\text{in}}} Im[\langle \chi_1 \rangle] + \frac{2\Gamma_L}{v_g I_{\text{in}}} \langle \chi_1^\dagger \chi_1 \rangle, \tag{2.31}$$

where χ_1 is b_1 for the direct-coupled qubits medium. We have explicitly verified numerically that $\mathscr{T}^{\infty}_{\text{THLE}} + \mathscr{R}^{\infty}_{\text{THLE}} = 1$.

2.3.5 The self-consistent mean-field analysis

The propagation of photons through the medium can also be studied using the mean-field approximation applied on the on-site interaction term in the Hamiltonian. In the case of direct-coupled qubits, after applying the mean-field approximation the Hamiltonian of the the medium becomes

$$H^{mf}_{direct} = \hbar \sum_{j=1}^{N} \omega_{q_j} b_j^\dagger b_j + U b_j^\dagger b_j (\langle b_j^\dagger b_j \rangle - 1) + \hbar \sum_{j=1}^{N-1} 2J_x (b_j^\dagger b_{j+1} + b_{j+1}^\dagger b_j). \tag{2.32}$$

The bath and bath coupling terms are also included in the complete Hamiltonian of the medium. To obtain the mean-field equations for the system, we derive a set of N equations by using the Heisenberg equations for the operators b_j for each site given by

$$\dot{b_j} = -(i\delta\omega_{q_j} + \Gamma_j) b_j - iU(\langle b_j^\dagger b_j \rangle - 1) b_j - 2iJ_x (b_{j-1} + b_{j+1}) - i\Omega_L \delta_{1,j}, \tag{2.33}$$

where, $\Gamma_j = 0$ for $2 \leq j \leq N-1$, $\Gamma_1 = \Gamma_L$ and $\Gamma_N = \Gamma_R$. If $N = 1$, $\Gamma = \Gamma_L + \Gamma_R$. We use open boundary condition for the medium, i.e. $b_0 = b_{N+1} = 0$. Similar to the quasi-classical equations, the mean-field equations have no dependence on other excited states and, therefore, N mean-field equations have all the necessary information to model the medium.

By comparing the Eq. 2.33 with the quasi-classical equations, we observe that the on-site interaction term in mean-field equations has missed a factor of 2 and has an additional -1 as well. Therefore, we put the factor of 2 in the on-site interaction and remove -1 explicitly in the numerical calculations.

Each of the mean-field equations has number operator ($\langle b_j^\dagger b_j \rangle$) in the RHS. Therefore to solve these equations at steady-state, we multiply each of the N equations with its conjugate to derive a set of coupled equations for number operators at each site. For example, we get the following self-consistent mean-field equations for a medium two direct-coupled qubits

$$\langle b_1^\dagger b_1 \rangle = \frac{|\delta\omega_{q_2} + 2U\langle b_2^\dagger b_2 \rangle - i\Gamma_R|^2 \Omega_L^2}{|4J_x^2 - (\delta\omega_{q_1} + 2U\langle b_1^\dagger b_1 \rangle - i\Gamma_L)(\delta\omega_{q_2} + 2U\langle b_2^\dagger b_2 \rangle - i\Gamma_R)|^2}, \tag{2.34}$$

$$\langle b_2^\dagger b_2 \rangle = \frac{4J_x^2 \Omega_L^2}{|4J_x^2 - (\delta\omega_{q_1} + 2U\langle b_1^\dagger b_1 \rangle - i\Gamma_L)(\delta\omega_{q_2} + 2U\langle b_2^\dagger b_2 \rangle - i\Gamma_R)|^2}. \tag{2.35}$$

In order to get numerical solutions of these equations we run a self-consistent loop over the set of equations for a large number of iterations and calculate the output transmission using the formula

$$\mathscr{T}_{mf}^{\infty} = \frac{2\Gamma_R}{v_g I_{\text{in}}} \langle b_N^\dagger b_N \rangle. \tag{2.36}$$

As mentioned before, the self-consistent mean-field after making the corrections mentioned above agrees with QCA for a wide range of parameters.

2.4 Results

For the direct-coupled array of N qubits, we calculate the steady-state solutions using THLE, QCA and modified QCA. We first set $v_g = 1$ and measure various parameters in units of qubit frequency ω_a. We assume all qubits in their ground state before irradiation with the photons, i.e. $\mathscr{S}(t \to t_0) = 0$ and $\beta_j(t \to t_0) = 0$. We use the steady-state solutions of Eqs. 2.16 and 2.17 to obtain the steady-state transmission probabilities: $\mathscr{T}_{\text{THLE}}^{\infty}$ and $\mathscr{T}_{\text{QCA}}^{\infty}$. For the modified QCA we replace the on-site interaction U with U_{eff} and obtain the transmission probability $\mathscr{T}_{\text{MQCA}}^{\infty}$.

We show in Fig. 2.1 the steady-state transmission for a single qubit and a pair of two directly coupled qubits using THLE, QCA and modified QCA analyses. For both single qubit and two direct-coupled qubit mediums, all the transmission results are calculated with maximum six bosons per qubit ($m = 6$) for the THLE analysis. For a single qubit, we show the transmission profiles, i.e. $\mathscr{T}_{\text{THLE}}^{\infty}$, $\mathscr{T}_{\text{QCA}}^{\infty}$ and $\mathscr{T}_{\text{MQCA}}^{\infty}$ versus scaled frequency ω_p/ω_a for different input intensities (I_{in}) in Fig. 2.1(a,d,g). At low input intensity, the three analyses, agree completely with each other.

The decrease in maximum transmission due to photon blockade, at resonant input frequency $\omega_p = \omega_a$, is more clear in Fig. 2.1(j), where we show lowering of transmission with increasing intensity. The reduction of transmission at very high light intensities is due to the saturation of qubits by photons, which completely blocks any transmission of light to the other end. This results in no interaction between the remaining photons. The observed decrease in the QCA transmission is due to the shifting of the transmission profile, and as mentioned before there is always some frequency with perfect transmission in this analysis, Fig. 2.1(m-o). We show the systemic variation of the entire transmission profile with intensities in Fig. 2.1(m,p,s) for QCA, THLE and modified QCA respectively. We observe that in all the single qubit transmission results, the QCA fails to match the THLE analysis, while the modified QCA has perfect agreement with THLE results for a large range of I_{in}.

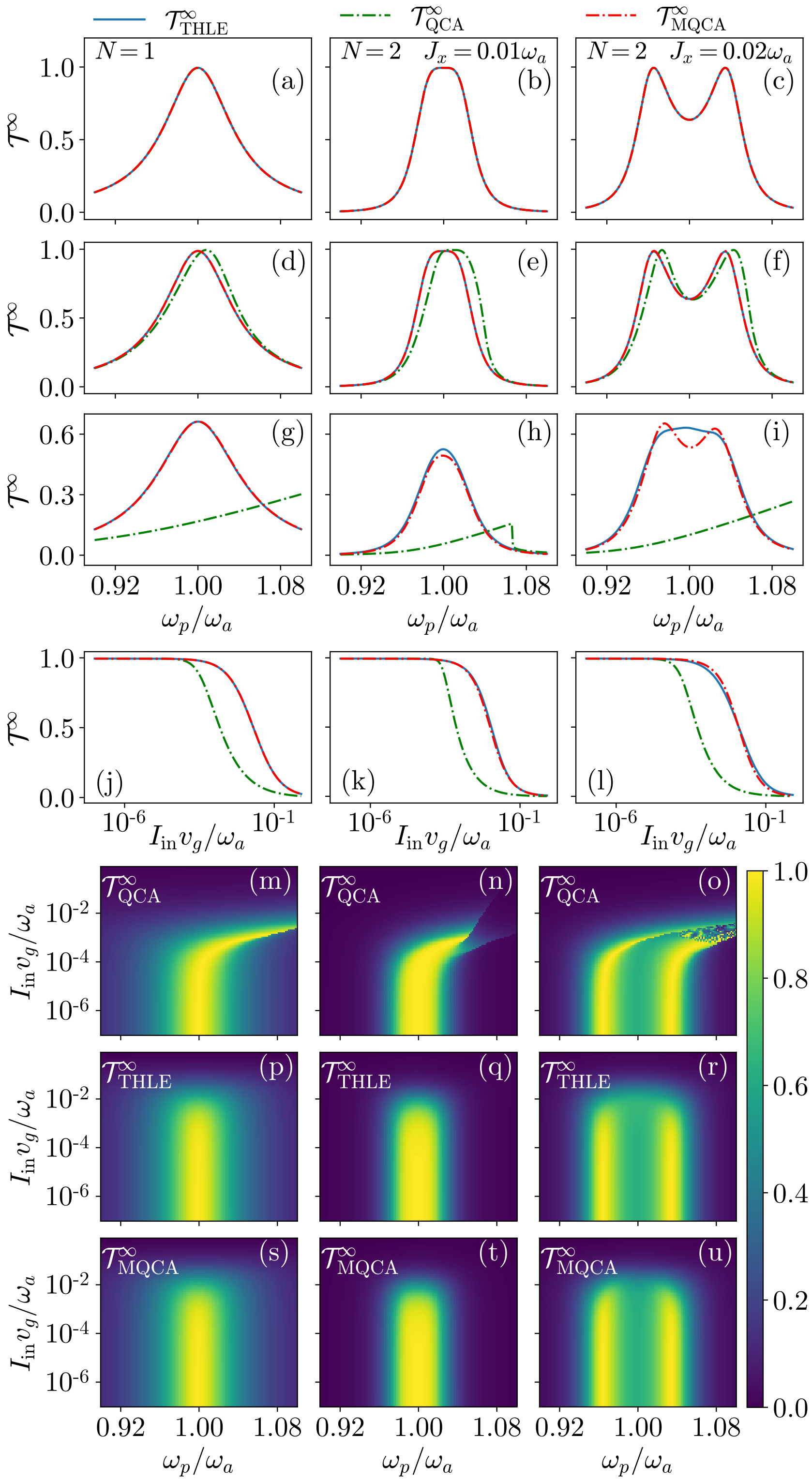

Fig. 2.1 (Caption on next page.)

Fig. 2.1 Single and two direct-coupled qubits steady-state transmission results comparing between the THLE ($\mathscr{T}^{\infty}_{\mathrm{THLE}}$), quasi-classical ($\mathscr{T}^{\infty}_{\mathrm{QCA}}$) and modified QCA ($\mathscr{T}^{\infty}_{\mathrm{MQCA}}$) analyses. First column shows transmission results for a single qubit while the other two columns show transmission results for two direct-coupled qubits at different values of $J_x = 0.01\omega_a$ and $J_x = 0.02\omega_a$. The first three rows show the effect of increasing the input intensity I_{in} (in terms of ω_a/v_g) of photons as $I_{\mathrm{in}} = 1.12\times10^{-6}$(a,b,c), $I_{\mathrm{in}} = 1.5\times10^{-4}$(d,e,f) and $I_{\mathrm{in}} = 0.01$(g,h,i). The fourth row shows transmission with increasing I_{in} at $\omega_p = \omega_a$(j,k) and $\omega_p = 0.965\omega_a$(l). The last three rows show variation in transmission profile for a range of I_{in} for the QCA, THLE and modified QCA analyses respectively. Other parameters are: $\omega_{q_1} = \omega_{q_2} = \omega_a$, $\Gamma_L = \Gamma_R = 0.02\omega_a$, $U = 1.05\omega_a$.

In the second and third columns of Fig. 2.1, we present the results for two directly coupled qubits at different inter qubit coupling strengths (J_x). In the second column, which has low inter qubit coupling strength ($2J_x = \Gamma_L = \Gamma_R$), we observe a single peak in the low intensity transmission profile, which is, in-fact due to the overlapping of the two peaks appearing at resonance for the two qubits in the system, Fig. 2.1(b). In the last column, we increase J_x ($J_x = \Gamma_L = \Gamma_R$), which shifts the resonance peaks away from each other and we observe the two peaks separately, Fig. 2.1(c). Again, for both QCA and modified QCA at low intensity two peaks appear but at high intensity they disappear.

We want to stress that U_{eff} is calculated by considering only single qubit and no additional fitting has been done, and still the modified QCA has captured the transmission reduction due to photon blockade fairly accurately. However, there is larger disagreement between these two analyses as J_x is increased. Even with a few limitations, the modified QCA is able to capture the photon blockade effects predicted by the THLE analysis reasonably well for a large set of parameters. Transmission from the three analyses as function of I_{in} for two qubit model at different J_x is shown in Fig. 2.1(k,l), where the transmission decreases with increasing I_{in}. We see a slightly larger disagreement between THLE and modified QCA transmission at higher J_x. The overall variation in transmission profile of the QCA, THLE and modified QCA with intensity can be seen by comparing the last three rows of Fig. 2.1, which shows the shift in the QCA transmission similar to the single qubit and the effectiveness of the modified QCA in matching the THLE transmission results.

We further show a comparison of the transmission profiles for the three analyses for upto five directly coupled qubits in Fig. 2.2. The three columns in Fig. 2.2 correspond to increasing system sizes of three, four and five qubits for the direct-coupled qubits medium. In the THLE analysis, the three, four and five direct-coupled qubits array have truncations at $m = 5, 3$ and 2 respectively. The truncation is larger, i.e. m decreases, for larger system sizes due to the computational capacity being reached. However, due to large on-site interaction U,

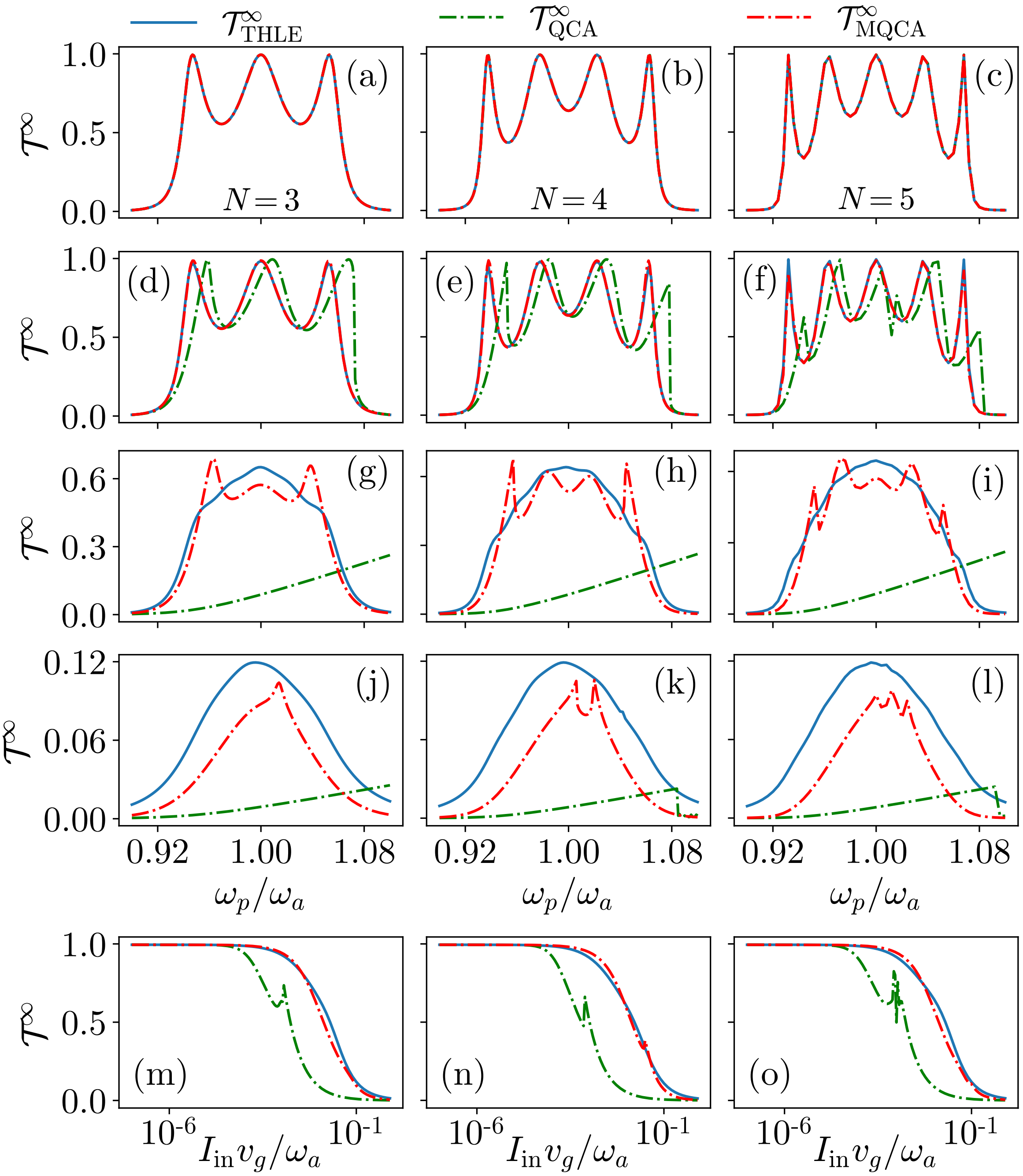

Fig. 2.2 Longer direct-coupled system steady-state transmission for the THLE ($\mathscr{T}^{\infty}_{\mathrm{THLE}}$), quasi-classical ($\mathscr{T}^{\infty}_{\mathrm{QCA}}$) and modified QCA ($\mathscr{T}^{\infty}_{\mathrm{MQCA}}$) analyses. The three columns show transmission profiles for system sizes (N) of 3, 4, and 5 qubits respectively. In the first four rows we show transmission profiles with input intensity I_{in}(in terms of ω_a/v_g) increasing on going down the columns as $I_{\mathrm{in}} = 1.12\times10^{-6}$(a,b,c), $I_{\mathrm{in}} = 1.5\times10^{-4}$(d,e,f), $I_{\mathrm{in}} = 0.01$(g,h,i) and $I_{\mathrm{in}} = 0.1$(j,k,l). The last row shows transmission with intensity at input frequency $\omega_p = \omega_a$ for $N = 3, 5$(m,o) and $\omega_p = 0.978\omega_a$ for $N = 4$(n). The remaining parameters are, $\omega_{q_j} = \omega_a$, $\Gamma_L = \Gamma_R = 0.02\omega_a$, $J_x = 0.02\omega_a$, $U = 1.05\omega_a$.

we expect the truncation errors to be negligible though we cannot check this explicitly for the largest system size. In the first four rows, we show the transmission profile with increasing I_{in} down the column. At low I_{in}, Fig. 2.2(a,b,c), we observe perfect resonant transmission with the number of peaks in the THLE transmission profile increase as resonance points increases with the system size. As the I_{in} is increased, similar to the single and two direct-coupled qubits case in Fig. 2.1, the THLE transmission profile shows the effect of photon blockade as maximum transmission decreases with I_{in}, Fig. 2.2(d,e,f). On further increase in I_{in}, the transmission further decreases and the peaks disappear in the THLE analysis, Fig. 2.2(g,h,i).

2.5 Conclusion

In this chapter, we have explored the transmission properties of photons through a lattice of direct-coupled qubits, where the qubits have on-site interaction. With the increase in intensity of incoming photons in a coherent state, the lattice develops effective photon-photon interactions and related photon blockade mediated by the on-site interaction at the qubits. For the lattice, at single photon limit the transmission line-shape shows resonance peaks equal to the number of qubits in the system. With an increase in intensity the photon blockade occurs, which causes lowering of resonance transmission peaks until negligible transmission is observed at a very high intensity when the qubits get saturated by photons.

We performed a quasi-classical analysis (QCA) for the lattice, which completely fails to show any transmission reduction due to photon blockade. It shows agreement with truncated Heisenberg-Langevin equation (THLE) at single particle limit but fails at higher intensities and shows a shift in the QCA transmission profile. One of our main contributions is to modify the QCA equations by introducing a complex on-site interaction by matching the THLE and QCA transmissions for the single site case. The modified QCA is successful in capturing effective photon-photon interactions for a wide range of parameters even at larger system sizes.

At low input intensity, both QCA and modified QCA matches the THLE transmission profile. However, as we increase the intensity, the on-site interaction at the qubits creates effective interactions or optical nonlinearities between photons mediated by the qubits' excitations cause photon blockade resulting in reduction of transport of photons, which is observed in the THLE transmission profile. The QCA only shows a shift in the transmission profile while the modified QCA agrees with the THLE results.